Hindawi
Shock and Vibration
Volume 2022, Article ID 3056354, 14 pages
https://doi.org/10.1155/2022/3056354

Research Article

Influence of Traction Motor Components on Thermal Characteristics of Traction Motor Bearings

Zhihong Bian,[1] Tingting Wang ,[2] and Dongli Song[3]

[1]*National Energy Railway Equipment Co., Ltd., Beijing, China*
[2]*School of Automation, Chengdu University of Information Technology, Chengdu, China*
[3]*State-Key Laboratory of Traction Power, Southwest Jiaotong University, Chengdu, China*

Correspondence should be addressed to Tingting Wang; wtt@cuit.edu.cn

Received 12 September 2022; Revised 22 October 2022; Accepted 29 October 2022; Published 21 November 2022

Academic Editor: Paolo Pennacchi

The operating temperature and thermal stress play key roles in overall performance of a cylindrical roller bearing used in high-speed train traction motor. The cylindrical roller bearing studied in this paper is in the housing of the traction motor. Due to the heating of each component of the traction motor, a thermal environment is formed in the housing that changes the temperature and stress of the traction motor bearing. In this paper, a thermal-mechanical coupled model of bearing considering the stator, rotor, and shaft was established to study the temperature and thermal stress of traction motor bearing. Experiments were conducted on a service high-speed train to validate the proposed bearing thermal analysis model, meanwhile, the temperature of the measurement point was revised by the theory of heat transfer. The revised experiment results show that the established thermal-mechanical coupled model is reasonable and effective. The results show that the heating of the stator and rotor of the traction motor has a great influence on the temperature and stress of the cylindrical roller bearing of the traction motor. When the heating of the stator and rotor is considered, the temperature of inner ring near the traction motor is higher than that of far away from the traction motor, and the overall temperature of each component of the bearing also increases. As for the stress, when the traction motor stator and rotor is considered, the maximum stress increases by 66.9%. Therefore, the heating of the stator of the traction motor must be considered when the thermal characteristics analysis and reliability analysis are carried out on the cylindrical roller bearing.

1. Introduction

Cylindrical roller bearing used in motor car traction motor is a key component for ensuring safe operation of high-speed train, it is also one of the most vulnerable parts of the motor. The cylindrical roller bearing of traction motor of high-speed train has high running speed and harsh service environment. In the service process, the friction heat of the bearing will increase sharply, resulting in excessive temperature of the bearing. If there is no effective cooling, it will cause raceway burns of raceways and bearing lubrication failure, as shown in Figure 1. Once failure of a motor car traction motor bearing, it may lead to serious accidents [1]. Therefore, it is necessary to analyze the thermal characteristics of cylindrical roller bearing under the thermal field environment of traction motor of high-speed train to guide the design, optimum, and monitoring of bearing during its operation in high-speed train.

The traction motor cylindrical roller bearing of high-speed train is affected by both mechanical load and temperature when the bearings are used in the vibration environment of high-speed trains and the thermal field environment of traction motors. The thermal expansion deformation caused by the temperature difference of the bearing surface and the elastic deformation of the bearing surface are almost at the same magnitude, which have a great influence on the bearing stress field. Meanwhile, the stress field inside the bearing is the key factor for strength design and failure mechanism analysis. Thermal stress analysis is a thermodynamic coupling problem involving temperature

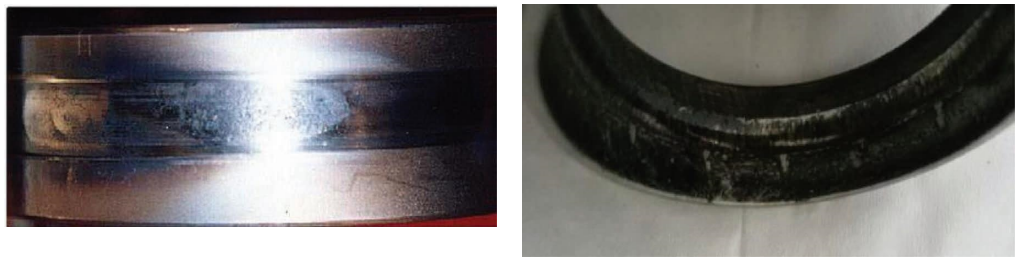

(a) (b)

Figure 1: Bearing damage caused by thermal effect. (a) Bum of inner raceway. (b) Lubrication failure.

field and stress field. In the process of analysis, the effect of each physical field and the influence of each other should be considered simultaneously. Therefore, thermal coupling analysis is required.

At present, the finite element method is mostly used to study the thermal analysis, such as Cao [2] and You [3]. Brown and Forster [4] calculated the friction heat of bearing with Gupta program and calculated the steady-state temperature field of each single element of angular contact ball bearing with ANSYS software. Xu et al. [5] established a three-dimensional finite element model for thermal deformation analysis of rolling bearings based on the principle of heat transfer and tribology. Overstam [6] performed finite element simulations using the MSC.MARC code to study the effect of bearing geometry on the residual stress-state in cold drawn wires. Tarawneh et al. [7, 8] analyzed the heat transfer paths inside the tapered roller bearings via the experimental and theoretical methods. Kletzli et al. [9] analysed the thermal failures in railroad class F($61/2 \times 12$) tapered-roller bearings operated at high speeds using the ABAQUS, which is a commercial finite element software and has been employed to analyze bearing temperature field distribution and its influence factors.

In addition to the study of the temperature field, some researchers have also studied the thermal stress. Chen [10] established a transient temperature field model of planetary gear bearing with ANSYS software and analyzed the thermal stress and thermal deformation of the bearing. You [11] established the transient thermal analysis model and the coupled thermal structure analysis model of high-speed motorized spindle bearing with ANSYS software, and analyzed the thermal deformation of the bearing at the rated speed. A thermal-mechanical coupling model was established by Lin et al. [12] based on finite element method, and the stiffness change induced by centrifugal effect was discussed. Zhou [13] used ANSYS software to analyze the heat-structure coupling of ceramic ball bearing mixed with high-speed and small composite molecular pump and obtained the bearing-related stress and deformation.

The railway track irregularity leads to all the components of train working in high-speed vehicle vibration environment, and an additional force will be imposed on the bearing by vehicle vibration environment, which accelerates the temperature rising of the bearing [14]. At the same time, the heating of the traction motor stator and rotor makes the cylindrical roller bearing of the traction motor in the thermal field environment. However, the research of thermal characteristics of bearings considering the heating of tractor motor stator and rotor have not been found until now.

Therefore, a thermal analysis model of bearing considering the heating of tractor motor stator and rotor is proposed in this paper to study the thermal characteristics of bearing servicing in high-speed train. Experiments are conducted on a service high speed train (i.e., CRH380B) to validate the proposed bearing thermal analysis model. The temperature and thermal stress of bearing under thermal field environment are attempted to be studied with the proposed bearing thermal analysis model. This study is anticipated to be theoretical support to the optimum design of cylindrical roller bearing used in motor car traction motor in high-speed train.

2. Modelling and Simulations

2.1. Bearing Parameters. The bearing used in traction motor nondrive end of high-speed train is cylindrical roller bearing. The structural parameters of this cylindrical roller bearing are shown in Table 1. The bearing is made with GCr15, and the material parameters are shown in Table 2.

2.2. Establishment of Thermal-Mechanical Coupled Model. To analyze the temperature distribution and thermal stress of traction motor bearing, a FE model is established by ABAQUS. Combined with the knowledge of thermoelastic mechanics and finite element discrete knowledge, finite element equation for dynamic thermo-mechanical coupled problem is shown in the following equation [15].

$$[M]\left\{\frac{\partial^2 \delta}{\partial t^2}\right\}_t + [K]\{\delta\}_t = \{F\}_t. \quad (1)$$

When the mechanical and thermal loads do not change dramatically with time, the displacement acceleration is very small and can be neglected, that is, the first term in equation (1) is 0. This method greatly simplifies the calculation process and is used in most engineering problems. In ABAQUS, most thermo-mechanical coupling units are calculated in this way. Therefore, the first term (dynamic term) in equation (1) is removed, the finite element equation can be obtained as follows:

Table 1: Geometric parameters of the cylindrical roller bearing.

Bearing outer ring diameter D (mm)	90
Bearing inner ring diameter d (mm)	50
Bearing width B (mm)	10
Roller diameter d_m (mm)	10
Number of rollers	19

$$[K]\{\delta\} = \{F\},$$
$$\{F\} = \{R\} + \{L\}, \tag{2}$$

where $\{L\}$ is thermal load vector, $\{R\}$ is force load vector, including concentrated force, surface force, and concentrated load.

From the point of view of finite element numerical calculation, the coupling effect of temperature field on the structure is only caused by the temperature load caused by the temperature change. Firstly, the steady-state temperature field of the structure is calculated, and then the temperature value of the discrete points are substituted into the finite element calculation equation as the load value. After calculating the displacement at that time, the relationship between displacement and strain and stress can be used to obtain the stress and strain at that time.

The ABAQUS/Standard coupled temperature-displacement solvers are adopted in the thermo-mechanical coupling model established in this paper. The validity of the FE model depends greatly on the correctness of the BCs applied when running the simulations. The BCs used for this study were derived from a well-established textbook in the field of heat transfer, and from material specifications provided by the bearing manufacturer. Three major BCs, which are described in this section, were utilized, namely, conduction, convection, and heat flux.

During the heat exchange of bearing parts, heat conduction will be conducted inside the outer ring, inner ring, and roller of the bearing. In addition, when the roller contacts with the inner and outer rings, heat conduction will also occur between each other. The heat conduction coefficients for the bearing assembly are provided by the bearing manufacturer. For the bearing steel, GCr15 with a thermal conductivity of 40 W/(m·K) was used. Convection BCs for the cylindrical roller bearing are calculated by the method provided in literature. The heat convection of bearing parts mainly includes two aspects: the heat convective between bearing parts and air (equation (3)) [16].

$$h_1 = \frac{0.175 K_f / R_i \sqrt{R_i \omega_i C/\nu \sqrt{C/R_i}}}{\ln\left(1 + C/R_i\right)}, \tag{3}$$

$$\begin{cases} h_2 = 0.03 \dfrac{K_f}{d}\left(\dfrac{u_r d}{\nu}\right)^{0.57}, & \text{force d heat convection,} \\ h_3 = 0.53 \dfrac{K_f}{D_o}\left(G_r P_r\right)^{0.25}, & \text{free heat convection,} \end{cases} \tag{4}$$

Table 2: Material parameters of the cylindrical roller bearing.

Density (t/mm^3)	7.8e − 9	Specific heat (mJ/t/k)	460e6
Young's Modulus (MPa)	207000	Expansion coefficient ($^\circ$C^{-1})	1.15e − 5
Poisson's ratio	0.3	Conductivity (mw/mm·k)	40

where K_f is thermal conductivity of lubricant or air, R_i is radius of inner raceway or outer raceway, ω_i is angular velocity of inner ring, C is distance between [17] the inside raceway and the outside raceway, ν is kinematic viscosity of lubricant, u_r is linear velocity of roller, G_r is Grushof number, and P_r is Prandtl number [18].

It can be seen from equation (1) that the mechanical load of bearing should be considered in addition to the thermal load when establishing the thermo-mechanical coupling model with ABAQUS. The weight of the rotor of the traction motor cannot meet the minimum load required by the bearing. To ensure the normal occlusion of the inner ring of the bearing and the rotor shaft, interference assembly is required when mounting the bearing. At this point, the inner ring of the bearing is subjected to a radial preload. According to literature [19], the calculation of the minimum radial load Frm (N) of cylindrical bearing is as follows:

$$F_{rm} = k_r\left(6 + 4\frac{n}{n_r}\right)\left(\frac{d_m}{100}\right)^2, \tag{5}$$

where k_r is minimum load factor, n is speed (r/min), n_r is reference speed (r/min), and d_m is pitch diameter (mm). The preload is at least 650 N when the bearing needs to operate at 3000 r/min.

The traction drive system of CRH380 train studied in this paper includes traction motor, gear drive system, and wheel set. The classic vehicle-track coupling dynamics model mainly includes vehicle system, track system, and wheel-rail coupling system. On this basis, the vehicle-track coupling dynamics model established in this paper adds traction drive subsystem, axle box bearing subsystem, and traction motor bearing system.

A random track irregularity measured from the Beijing–Tianjin high-speed rail line (in China) is adopted and shown in Figure 2(a). The traction transmission system comprises traction motor, gear transmission system, and wheelset. As shown in Figure 2(b), one end of the gear box is connected to bogie frame via elastic mounts and the other end is joined to the wheelset axle. Details of the bearing model are shown in Figure 2(c). When the running speed of high-speed train is 292 km/h, the radial force applied on bearing under the vehicle vibration environment calculated using the vehicle track dynamics model is established in the SIMPACK software [20], as shown in Figure 2. The force with a length of 1 s after stabilization is selected in the thermo-mechanical coupling model, as shown in Figure 3.

Finally, to simulate heat generation within the bearing assembly, heat flux is applied to the contact surface of the rollers and raceway. The value of heat flux is calculated based on friction loss and contact area. The specific calculation

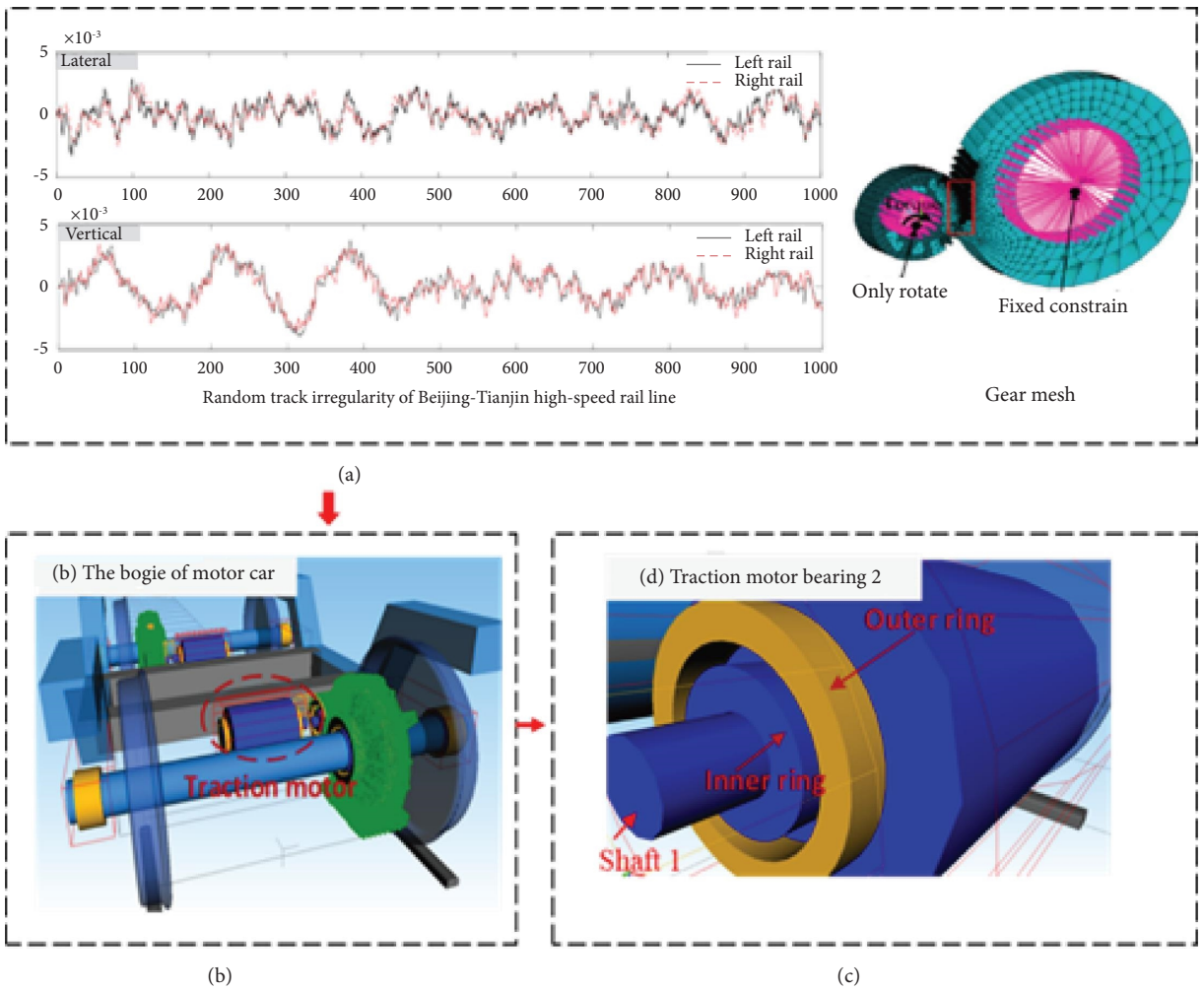

Figure 2: Vehicle dynamics model with motor car.

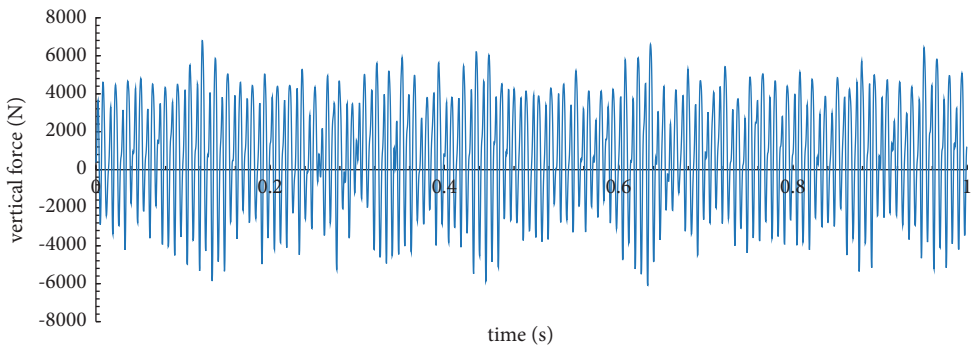

Figure 3: Bearing load due to vehicle environment.

process can be found in [21]. The heat flux of each component of bearing is shown in Figure 4.

In the service process of the motor, the internal energy exchange takes place. The iron loss, copper loss, mechanical loss, additional loss etc., generated will eventually be converted into heat energy, making each part of the motor hot. The iron loss P_{Fe}, copper loss P_{cu}, and mechanical loss P_{me} are calculated by the following equations:

$$P_{Fe} = K_a' P_{10/50} B^2 \left(\frac{f}{50}\right)^{1.3} G_c + K_a P_{Fe} G_e, \tag{6}$$

$$P_{cu} = mI^2 R, \tag{7}$$

$$P_{me} = 6.5\left(\frac{3}{p}\right)^2 (D_1)^3 \times 10^3, \tag{8}$$

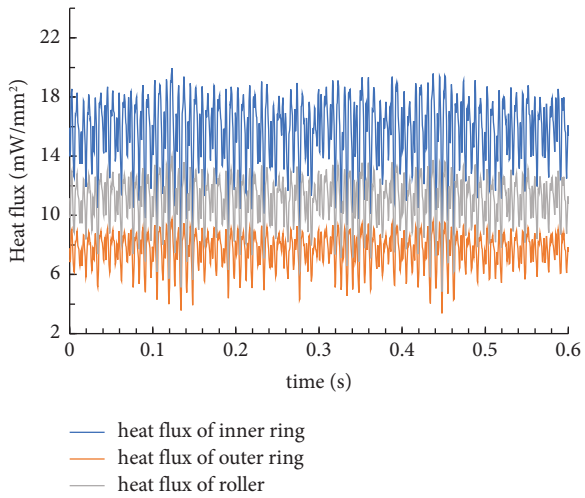

Figure 4: Heat flux applied on bearing.

where k_a and k_a' are empirical coefficient, $P_{10/50} = 2.0$ w; G_c and G_e are the weights of stator teeth and yoke cores, respectively; m is the number of phases and I is the current effective value of the stator winding, which refers to the resistance of each phase of the motor stator winding at the reference operating temperature; p is the pole number of the motor; and D_1 is the outer diameter of the motor, in mm.

The additional loss is difficult to calculate accurately and is generally selected according to production experience. According to literature [22], the additional loss is calculated as 1.5% of rated power for 4-pole motors with rated power greater than 11 kW.

When the traction motor operates at rated state, the iron loss, copper loss, mechanical loss, and additional loss generated are loaded on the corresponding parts of the traction motor, respectively. 70% of the iron loss is loaded on the stator core, 30% on the rotor core, 50% on the stator core, and the other 50% on the rotor core [23].

The energy loss of each component of the traction motor is shown in Table 3.

The power loss caused by the generation of heat since friction among bearing, calculated by the following equation, depends on the loads, bearing type and size, operating speed, properties, and quantity of the lubricant.

$$P = M\omega = M\frac{2\pi n}{60}, \tag{9}$$

where P is power loss caused by friction, in W; M is bearing friction torque, in N·mm; and n is rotating speed of bearing, in r/min.

The bearing friction torque M can be obtained according to the latest bearing friction torque calculation method of SKF. The detailed calculation procedures can be found in [24].

Figure 5 is the thermal-mechanical coupled model of the traction motor bearing with the traction motor. The heat transfer modes between each component of traction motor and bearing are as follows: (1) The heat of traction motor components is transmitted to the rotating shaft, then to the inner ring of bearing by the rotating shaft, and then to the roller of bearing and the outer ring of bearing by the heat exchange of lubricating oil. (2) The heat of each component of the traction motor is distributed to the surrounding air by means of convective heat transfer and heat radiation, so that the temperature of the surrounding air is increased, and then the ambient air temperature of the cylindrical roller bearing is changed. In this model, all the nodes on the inner surface of the inner ring of the traction motor bearing are coupled to the central control point of the inner ring. In the simulation analysis, the first step is to apply the time-varying heat flux on the rollers and raceway of inner ring and outer ring of the bearing. Thermal contact is established between the rotor shaft and the traction motor rotor core and between the shaft and the inner ring of the bearing. Second, to establish the radial load smoothly, apply a gravity load to the whole bearing, and let the contact pairs of the bearing slowly build up. The third step is to apply radial pretension at the control point of the inner ring. The fourth step is to apply the time-varying vibration load at the control point of the inner ring. Each component of the traction motor is defined as a rigid body to reduce the computation. All the nodes on the surface of each component are coupled to the control point of the rotor, and the translational and rotational degrees of freedom are fixed in each direction. The contact relationship between the inner ring raceway and roller, the outer ring raceway and roller, and the surface of the inner ring and the rotating shaft are defined, and the translation freedom and rotation freedom of the rotary shaft are constrained. The temperature of each component of the motor is transmitted to the inner ring of the bearing through the rotating shaft,

Table 3: The losses of each component of traction motor.

Part	Total loss (kW)	Volume loss (heat flux) (W·mm^{-3})
Stator core	2.3	0.02
Rotor core	1.5	0.016
Rotor coil	6.4	0.076
Stator coil	7.5	0.068

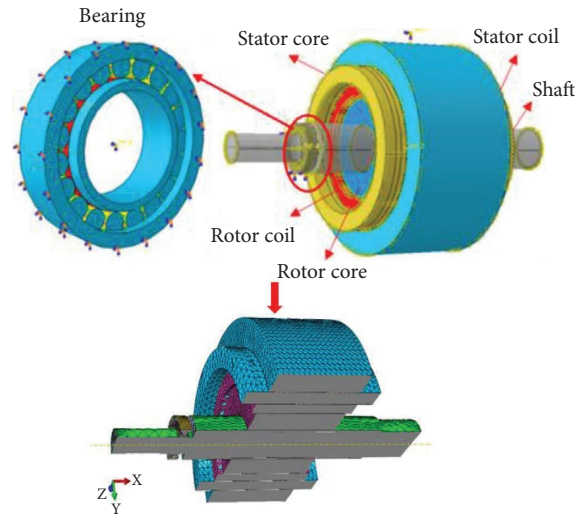

Figure 5: Thermal-mechanical coupled model of traction motor bearing considering other parts of the traction motor.

and then the temperature of the bearing roller and the outer ring is affected through the heat conduction between the solids. The thermal-mechanical coupled model of traction motor bearing shown in Figure 5 is meshed by tetrahedral elements with 109607 nodes and 219329 elements.

3. Experimental Measurement

To verify the established model, experiments were conducted on the high-speed train in service. The environment temperature, temperature of the traction motor bearings, and the running speed of high-speed train were monitored in real-time and recorded in vehicle wireless information transmission system. The arrangement of sensors is shown in Figure 6. Because the temperature sensor of the motor bearing is arranged on the outside of the motor housing, the measured bearing temperature is lower than the actual temperature. To verify the thermal analysis model of bearing, the actual temperature data need to be revised.

The heat exchange between outer ring of bearing and motor housing is simplified as shown in Figure 7, where the q is heat flux of inner surface of outer ring, the T_f is temperature of lubricant, T_{bi} is temperature of inner surface of outer ring, T_{bo} is temperature of outer surface of outer ring, T_{ho} is temperature of outer surface of bearing housing, T_a is temperature of air inside the motor housing, T_{si} is temperature of inner surface of motor housing, and T_{so} is temperature of outer surface of motor housing. It is assumed that the heat conduction of bearing outer ring and motor housing is one-dimensional steady state heat conduction. In the steady state condition, the heat generated from the inner surface of the outer ring must be completely lost to the surrounding fluid, and the heat transferred from the interface to the fluid is the same.

According to the laws of thermodynamics [25], at steady state, all the heat generated in the outer ring must be lost to the air. The following equation can be obtained from the thermal equilibrium:

$$\begin{aligned} q &= \frac{\lambda}{R_o}\frac{T_{ho}-T_{bo}}{\ln\left(R_h/R_o\right)}, \\ q &= h_b\left(T_{ho}-T_a\right), \\ q &= h_s\left(T_a-T_{si}\right), \\ q &= \frac{\lambda}{r_1}\frac{t_{si}-t_{so}}{\ln\left(r_2/r_1\right)}, \\ q &= \frac{\lambda}{R_{mi}}\frac{T_{si}-T_{so}}{\ln\left(R_{mo}/R_{mi}\right)}. \end{aligned} \tag{10}$$

The temperature difference between the outer surface of the bearing ring and the measuring point of the motor housing can be obtained as follows:

$$T_{bo}-T_{so} = \frac{q}{h_b}+\frac{q}{h_s}+\frac{q\left[R_{mi}\ln\left(R_{mo}/R_{mi}\right)-R_o\ln\left(R_h/R_o\right)\right]}{K_m}, \tag{11}$$

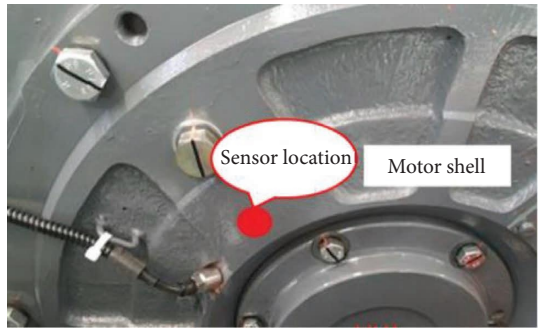

Figure 6: Bearing temperature sensor location.

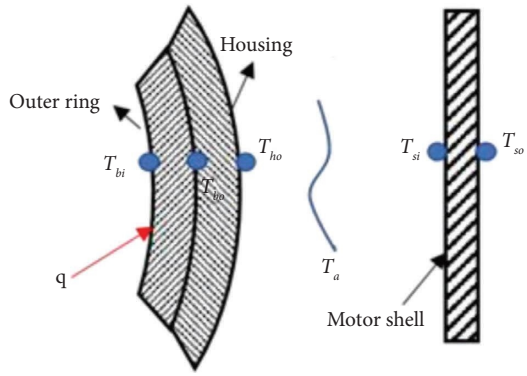

Figure 7: Simplified figure of heat exchange between bearing outer ring and motor housing.

where R_h is outside diameter of bearing housing, R_o is outside diameter of outer ring, R_{mi} is inside diameter of motor shell, R_{mo} is outside diameter of motor shell, h_b is heat convective coefficient between the outer surface of bearing housing and air, h_s is heat convective coefficient between the inner surface of motor shell and air, λ is heat conductivity of motor shell, and δ is thickness of motor shell.

Acceleration process (2017/3/1 6:40~2017/3/1 6:49) without coasting among the 12 hours is selected as the target process during which the speed accelerated from 0 to 292.07 km/h. The measured speed of high-speed train and bearing temperature are shown in Table 4.

4. Result and Analysis

4.1. Verification of the Bearing Thermal Analysis Model. The 6 levels of running speed of high-speed train, ambient temperature 19.14°C, the preload 650 N, and vertical load under vehicle environment (Figure 3) are used when simulating. The simulated temperature value of the bearing is taken as the temperature of the node 772 closest to the temperature sensor, which is the highest point along the Y-axis of the bearing outer ring of the traction motor. The comparison between simulation result and revised measurement result is given in Figure 8. It can be seen from Figure 8(a) that the variation trend of the simulated temperature value and the experimental temperature value with the speed is basically consistent. The simulation tolerance is about 9.5%~11.1%

Table 4: The measured speed of high-speed train and bearing temperature.

Time	Running speed (km/h)	Temperature of bearing (°C)	Environment temperature (°C)
6:40	23.37	19.14	19.14
6:41	40.63	19.14	
6:42	88.29	19.14	
6:43	180.68	20.27	
6:44	224.56	21.41	
6:45	251.19	22.55	
6:46	241.98	22.55	
6:49	292.07	23.69	

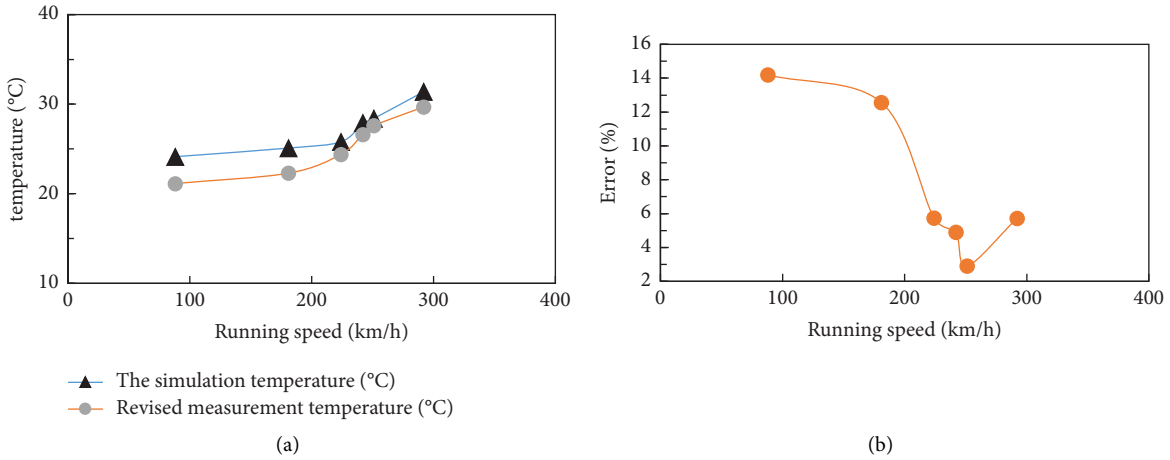

Figure 8: Comparison between the simulation results and experiment results: (a) trend of simulation temperature and measurement temperature and (b) error of simulation temperature and measurement temperature.

(Figure 8(b)), which is acceptable in engineering, indicates that the model is effective.

4.2. Temperature Distribution of Bearing considering the Heat of Tractor Motor Stator and Rotor. The whole temperature field of bearing is obtained with the proposed bearing model, as shown in Figure 9. Figure 9(a) is the cloud charts of temperature distribution of inner ring, outer ring, and roller, respectively, considering the heat of tractor motor. Figure 9(b) is the cloud charts of temperature distribution of inner ring, outer ring, and roller, respectively, without considering the heat of tractor motor stator and rotor.

As shown in Figure 9(a), the temperature of the bearing inner ring is no longer symmetrically distributed in the axial direction and the temperature near the traction motor is higher than that of far from the traction motor. This is because the temperature of the rotating shaft is highest in contact area with the motor rotor in the axial direction, and then decreases gradually to both sides. Therefore, the temperature of contact area with the inner ring near the motor side is higher than that of far from the motor side, and the heat transferred from the shaft to the inner ring is also higher near the motor side than that of far from the motor side.

It can be seen from Figure 9(a), the temperature of the bearing assembly considering heat of traction motor and rotor is higher than that of without considering the heat. For example, when the traction motor operates under rated working conditions, the maximum temperature of the bearing inner ring increases by 10.9°C, the maximum temperature of the bearing roller increases by 10.3°C, and the maximum temperature of the bearing outer ring is 6.7°C higher.

4.3. Thermal Stress of Bearing considering the Heat of Tractor Motor Stator and Rotor. The stress distribution of bearing considering the heat of tractor motor stator and rotor is shown in Figure 10. To show the maximum stress area more clearly, the stress lower limit value in the cloud chart is adjusted higher. It is observed that the maximum stress (281.5 MPa) is in the middle of the roller (Figure 10(b)). This is because that the temperature of the contact area between the inner ring and the outer ring is high, resulting in thermal expansion. When in contact with the roller, press against the roller, resulting in stress. The maximum equivalent stress (169.7 MPa) of the inner ring is located on the inner surface of the inner ring and not on the contact surface, which is consistent with the results in [26]. The temperature of the inner ring raceway is higher than that of other location and the linear expansion is large, while the inner surface of the inner ring is restrained and the longitudinal direction is weaker than that of other directions, so the linear expansion

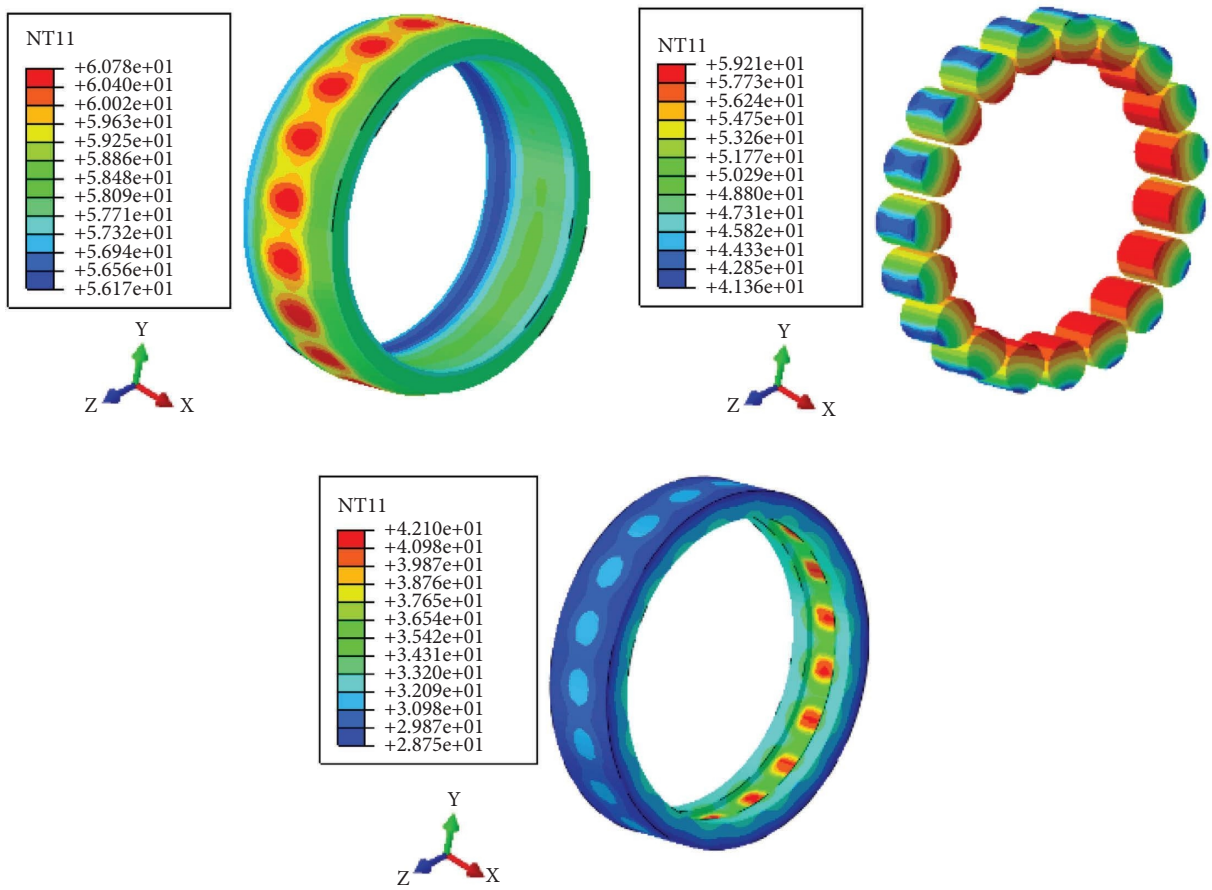

(a)

Figure 9: Continued.

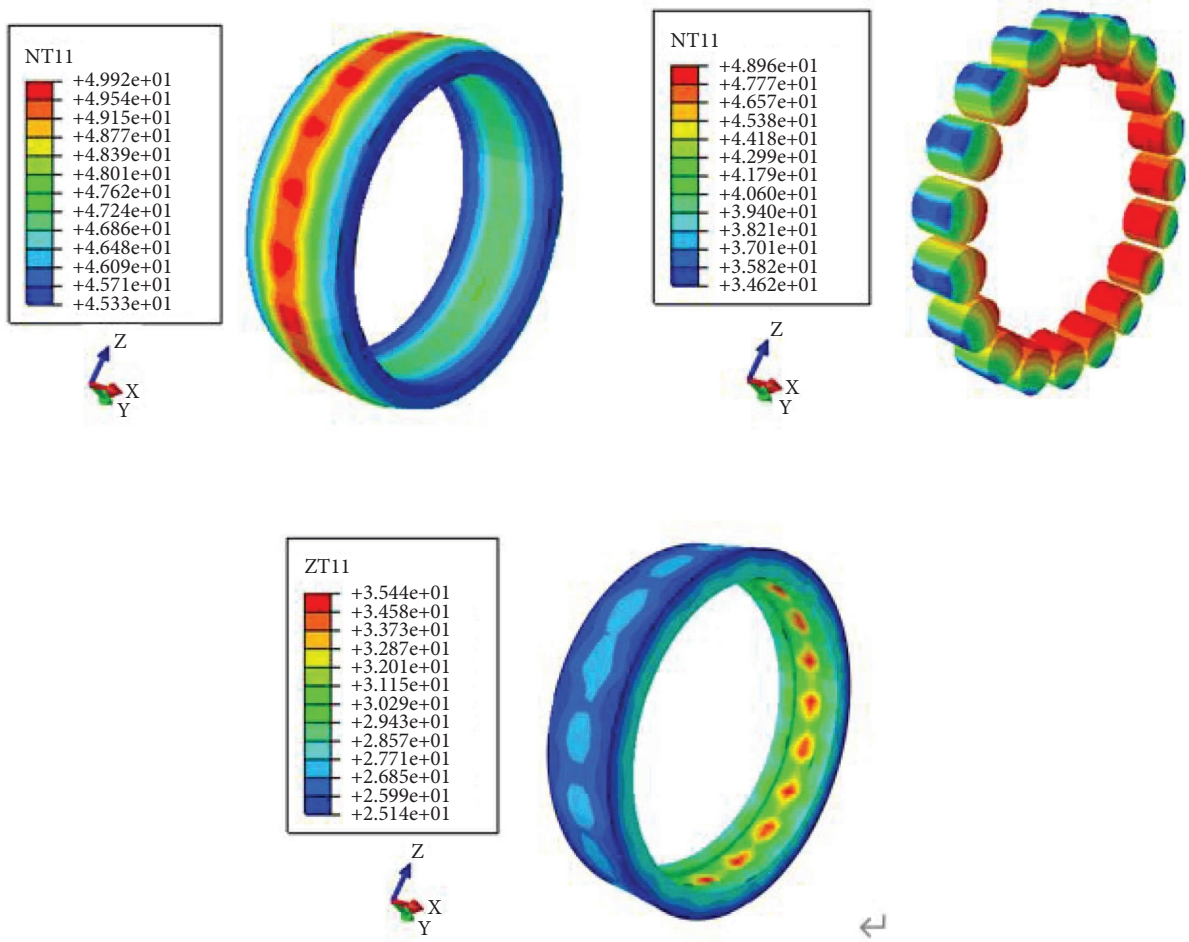

(b)

Figure 9: Bearing steady-state temperature distribution: (a) considering the heat of tractor motor and rotor and (b) without considering the heat of tractor motor and rotor.

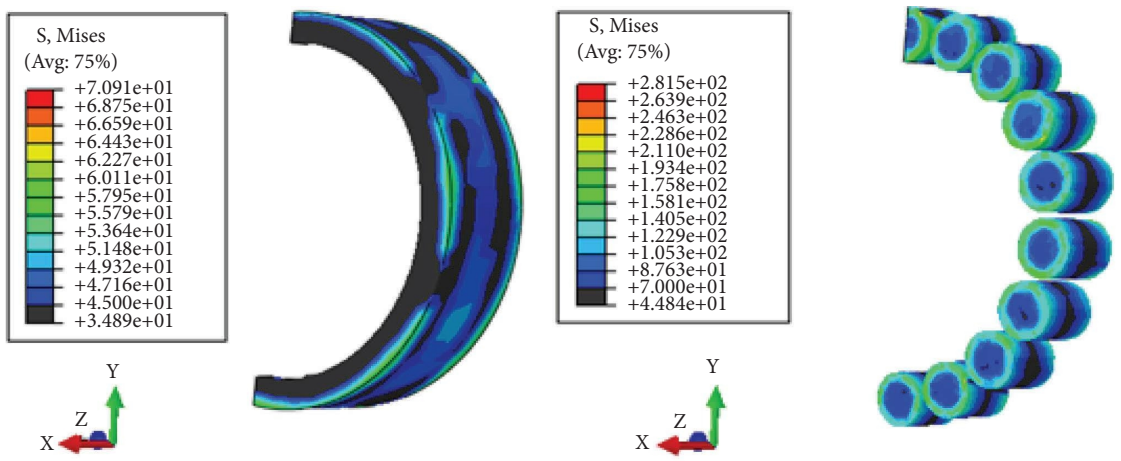

(a) (b)

Figure 10: Continued.

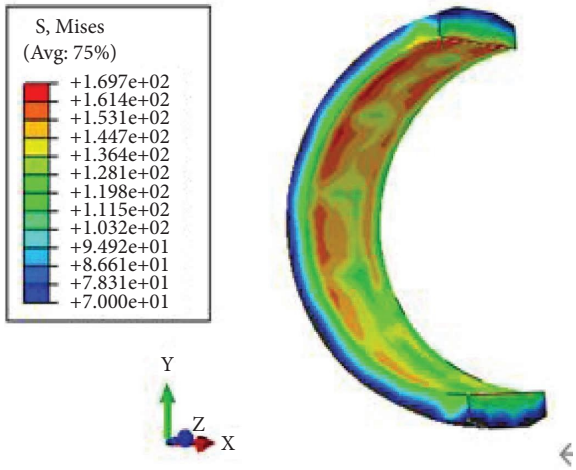

(c)

Figure 10: Bearing stress distribution (the unit is MPa).

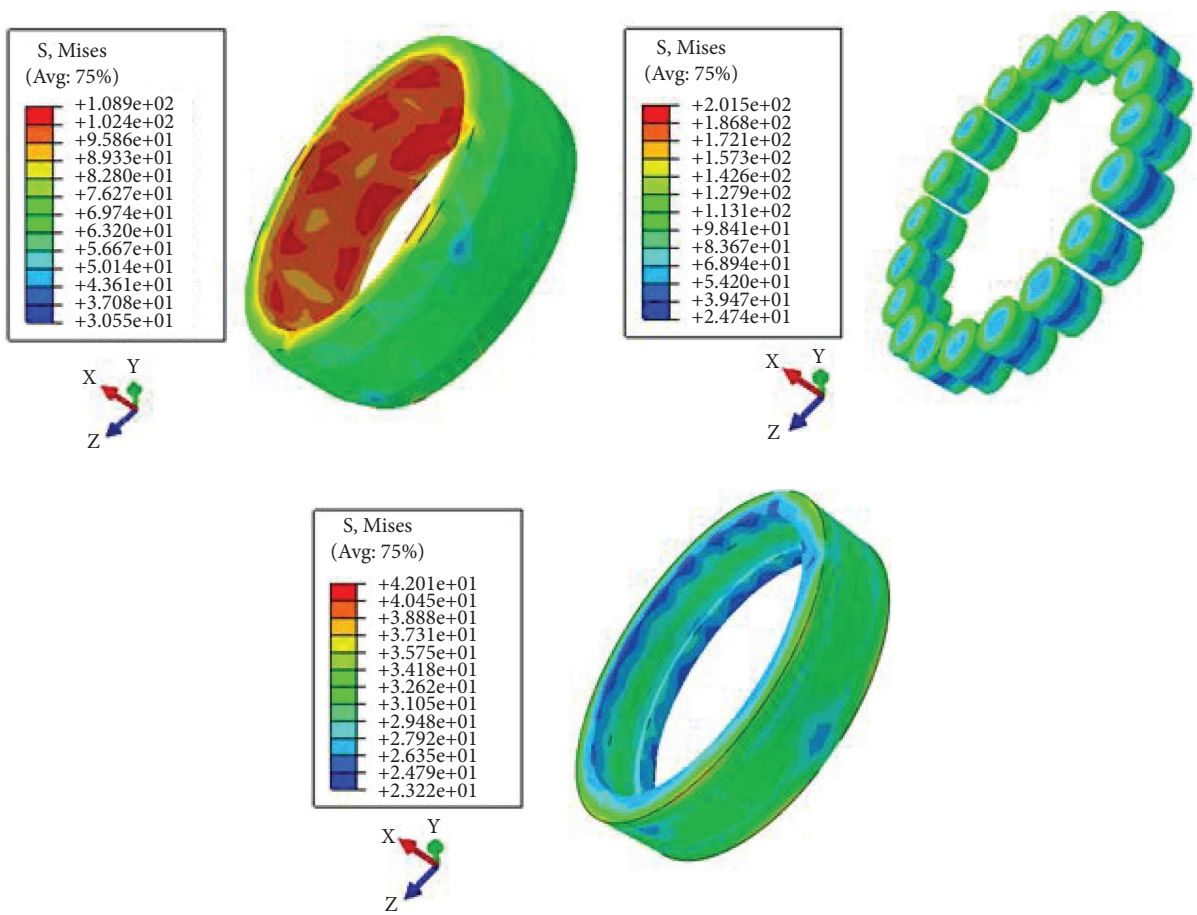

(a)

Figure 11: Continued.

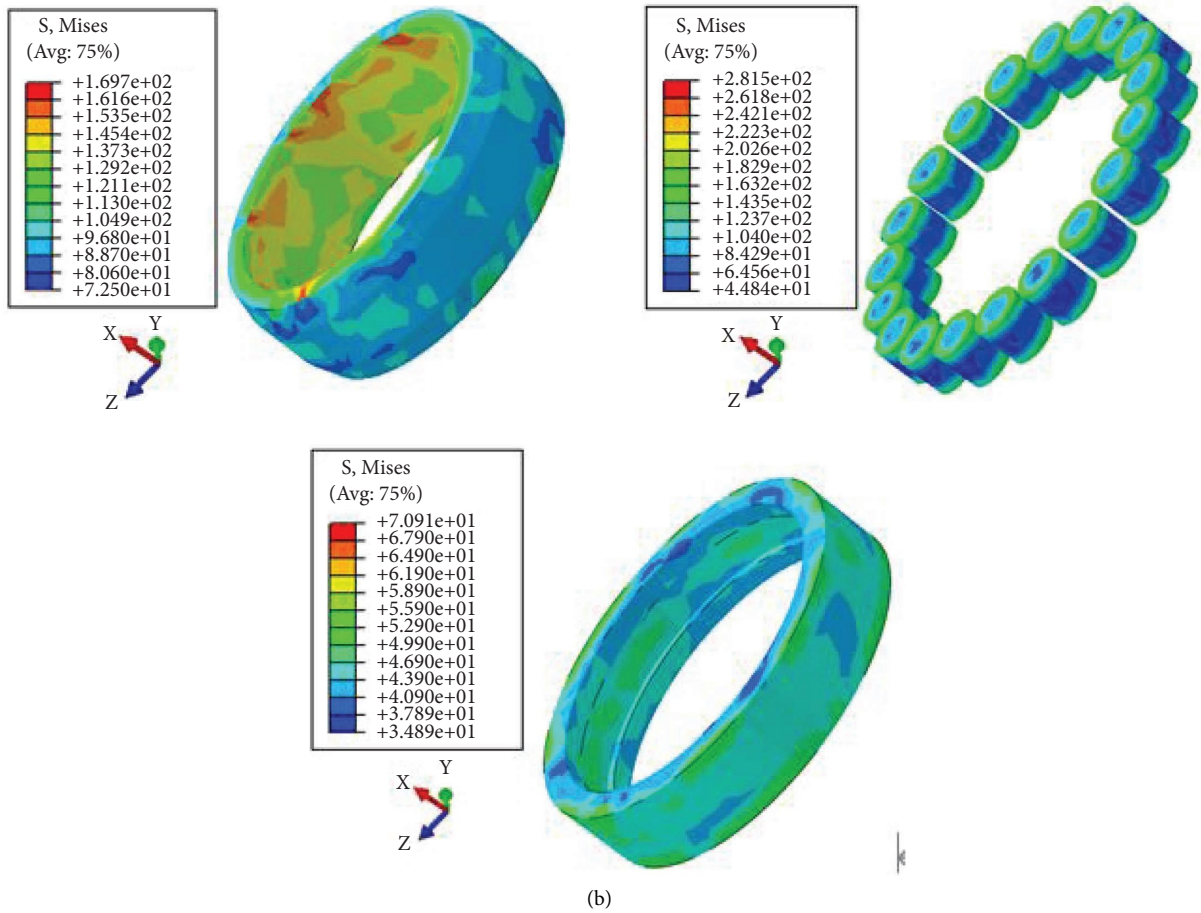

(b)

FIGURE 11: Thermal stress distribution of bearing: (a) without considering the heat of tractor motor stator and rotor and (b) considering the heat of tractor motor stator and rotor (the unit is MPa).

develops towards the inner surface of the inner ring. It can be observed from Figure 10 that the position of maximum stress is at the edge of the outer surface of the outer ring. For the outer ring, the position of maximum stress is at the edge of the outer surface of the outer ring. The constraint on the outer surface of the outer ring is stronger than other positions, while for the outer surface of the outer ring, the lateral constraint is weaker, so the linear expansion develops to the edge.

The comparison of thermal stress distribution with and without considering the heat of tractor motor stator and rotor is shown in Figure 11. It is shown that the heat of tractor motor stator and rotor has little influence on the thermal stress distribution of cylindrical roller bearing.

The comparison of the maximum physical field values of traction motor bearing considering the heating of tractor motor and not considering the heating of tractor motor is shown in Figure 12. It is shown that the heating has a great influence on the temperature field, displacement field, strain field, and stress field of the cylindrical roller bearing of traction motor. When the heat of traction motor rotor is considered, the maximum equivalent stress of bearing inner ring increases by 53 MPa (45.7%), outer ring by 28.4 MPa (66.9%), and roller by 75.4 MPa(36.7%).

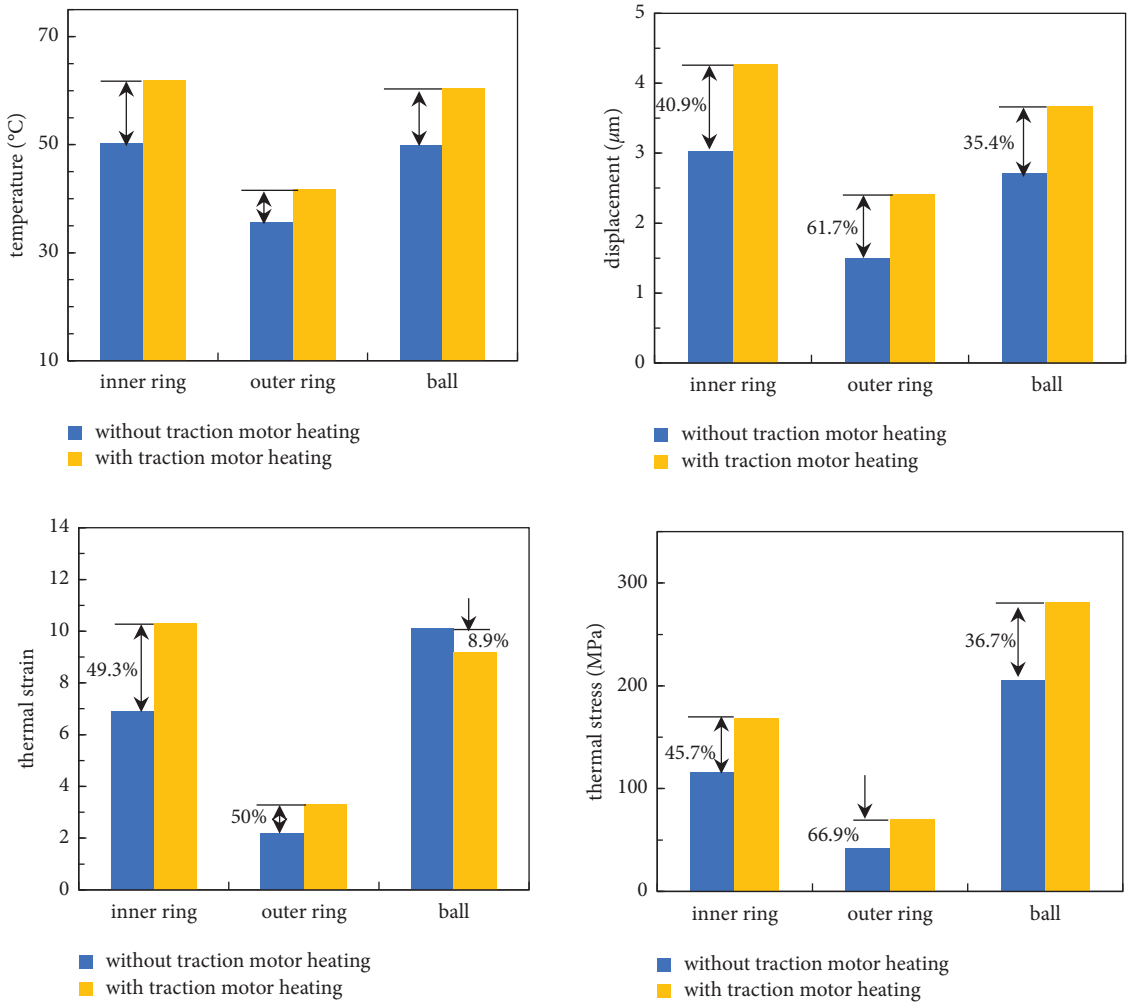

Figure 12: Comparison of thermal stress and comprehensive stress of traction motor bearing.

5. Conclusions

A thermal-mechanical coupled model of motor traction bearing considering the heating of the traction motor stator and rotor is proposed in this paper to study the effect of heating on the temperature distribution, thermal stress, and displacement of traction motor bearing. Experiments are conducted on high-speed train to validate the thermal-mechanical coupled model. The major findings of this study are summarized as follows:

(1) The heating of the traction motor stator and rotor has a significant influence on the thermal characteristics of the cylindrical roller bearing of traction motor in service in a high-speed train.

(2) The heating of traction motor stator and rotor affects the temperature distribution and temperature magnitude of the cylindrical roller bearing of traction motor. When the heating is considered, the maximum temperature can be increased by 10 degrees, and the temperature distribution is no longer symmetrical distribution.

(3) The heating of the traction motor stator and rotor has little influence on the stress distribution of the traction motor bearing, but has a great influence on the stress value. When the heating is considered, the maximum thermal stress can be increased by 66.9%.

Based on the above results, we know that the stator and rotor temperature of the traction motor have great influence on the temperature and distribution of the bearing, as well as the thermal stress. Therefore, we need to use the bearing temperature affected by the rotor temperature of the traction motor when evaluating the bearing life of the traction motor. And in engineering monitoring, we can choose monitoring points more accurately.

Nomenclature

D: Bearing outer ring diameter
d: Bearing inner ring diameter
B: Bearing width
d_m: Roller diameter
$[M]$: Mass matrix

$[K]$: Stiffness matrix
$[F]$: Force matrix
$\{L\}$: Thermal load vector
$\{R\}$: Force load vector
K_f: Thermal conductivity of lubricant or air
R_i: Radius of inner raceway or outer raceway
ω_i: Angular velocity of inner ring
C: Distance between the inside raceway and the outside raceway
v: Kinematic viscosity of lubricant
u_r: Linear velocity of roller
G_r: Gruschoff number
P_r: Prandtl number
F_{rm}: Minimum radial load of bearing
k_r: Minimum load factor
n: Speed of bearing
n_r: Reference speed of bearing
d_m: Pitch diameter of bearing
P_{Fe}: Iron loss
P_{cu}: Copper loss
P_{me}: Mechanical loss
k_{a}, k_a': Empirical coefficient
G_{c}, G_{e}: Weights of stator teeth and yoke cores, respectively
m: Number of phases
I: Current effective value of the stator winding
p: Pole number of the motor
D_1: Outer diameter of the motor
R_h: Outside diameter of bearing housing
R_o: Outside diameter of outer ring
R_{mi}: Inside diameter of motor shell
R_{mo}: Outside diameter of motor shell
h_b: Heat convective coefficient between the outer surface of bearing housing and air
h_s: Heat convective coefficient between the inner surface of motor shell and air
λ: Heat conductivity of motor shell
δ: Thickness of motor shell.

Data Availability

All data generated or analyzed during this study are included in the article.

Disclosure

The results and opinions presented are those of the authors and do not necessarily reflect those of the sponsoring agencies.

Conflicts of Interest

The authors declare that they have no conflicts of interest.

Acknowledgments

This research was sponsored by the Shenhua Group (Grant No. SHGF-17-54). These supports are gratefully acknowledged.

References

[1] Z. Y. Zhang, "Fault analysis and diagnosis of traction motor of high-speed train," *Internal Combustion Engine & Parts*, vol. 290, no. 14, pp. 173-174, 2019.
[2] J. Cao, *The Research on Thermal Character of HTM850G Machine Tools System*, Zhejiang University, Hangzhou, China, 2008.
[3] J. You, *Thermal Performance Analysis and Optimization of Motorized Spindle*, Huazhong University of Science and Technology, Wuhan, China, 2011.
[4] J. Brown and N. Forster, "Operating temperatures in lubricated rolling element bearings for gas turbines," *AIAA-2000-3027*, pp. 1268–1275, 2000.
[5] J. Xu, W. Qu, and N. Zhao, "Analysis on temperature field and thermal deformation of rolling bearings," *Bearing*, no. 5, pp. 1–3, 2006.
[6] H. Overstam, "The influence of bearing geometry on the residual stress state in cold drawn wire, analysed by the FEM," *Journal of Materials Processing Technology*, vol. 171, no. 3, pp. 446–450, 2006.
[7] C. M. Tarawneh, K. D. Cole, B. M. Wilson, and F. Alnaimat, "Experiments and models for the thermal response of railroad tapered-roller bearings," *International Journal of Heat and Mass Transfer*, vol. 51, no. 25–26, pp. 5794–5803, 2008.
[8] C. M. Tarawneh, A. A. Fuentes, J. A. Kypuros, L. A. Navarro, A. G. Vaipan, and B. M. Wilson, "Thermal modeling of a railroad tapered-roller bearing using finite element analysis," *Journal of Thermal Science and Engineering Applications*, vol. 4, no. 3, Article ID 031002, 2012.
[9] D. B. Kletzli, C. Cusano, and T. F. Conry, "Thermally induced failures in railroad tapered roller bearings," *Tribology Transactions*, vol. 42, no. 4, pp. 824–832, 1999.
[10] L. Chen, *Analysis of Temperature Field of Planetary Gear Reducer Based on ANSYS*, Nanjing University of Aeronautics and Astronautics, Nanjing, China, 2009.
[11] J. You, *Analysis and Optimization of Thermal Performance of High-Speed Motorized Spindle*, Huazhong University of Science and Technology, Wuhan, China, 2011.
[12] C. W. Lin, J. F. Tu, and J. Kamman, "An integrated thermo-mechanical-dynamic model to characterize motorized machine tool spindles during very high speed rotation," *International Journal of Machine Tools and Manufacture*, vol. 43, no. 10, pp. 1035–1050, 2003.
[13] H. P. Zhou, *Hybrid Ceramic Ball Bearing thermal Analysis of High-Speed Small Composite Molecular Pump*, Southwest University of Science and Technology, Mianyang, China, 2016.
[14] L. S. Ge, *Research on Dynamic Behavior of Axle Box Bearings of High-Speed Trains*, Southwest Jiaotong University, Chengdu, China, 2016.
[15] H. G. Wang, *Introduction to Thermoelastic Mechanics*, Tsinghua University Press, Beijing, China, 1989.
[16] J. H. Rumbarger, E. G. Filetti, and D. Gubernick, "Gas turbine engine main shaft roller bearing system analysis," *Journal of Lubrication Technology*, vol. 95, no. 4, pp. 401–416, 1973.
[17] E. R. G. Eckert, *Introduction to the Transfer of Heat and Mass*, McGraw-Hill, New York, NY, USA, 1950.
[18] G. C. Chen, *Thermal Analysis of High-Speed Rolling Bearing Used in Main Shaft of Aeroengine*, Harbin Institute of technology, Harbin, China, 2008.
[19] Z. Z. Wu and L. M. Wu, *Machine Design*, China Railway Publishing House, Beijing, China, 2016.

[20] B. R. Miao, R. Luo, and Z. Wang, *Advanced Tutorial on SIMPACK Dynamics Analysis*, Southwest Jiaotong University Press, Chengdu, China, 2010.
[21] T. T. Wang, Z. W. Wang, D. L. Song, W. Zhang, J. Li, and D. Chen, "Effect of track irregularities of high-speed railways on the thermal characteristics of the traction motor bearing," *Proceedings of the Institution of Mechanical Engineers - Part F: Journal of Rail and Rapid Transit*, vol. 235, no. 1, pp. 22–34, 2020.
[22] L. N. Li, B. L. Wang, and R. H. Zhou, *Motor Design*, Tsinghua University Press, Beijing, China, 1992.
[23] D. J. Li, *Analysis and Calculation of Generator Heat and its Application*, pp. 57–59, Sichuan University Press, Chengdu, China, 1994.
[24] Skf, *SKF Rolling Bearings General Catalogue*, SKF, Gothenburg, Sweden, 2013.
[25] S. M. Yang and W. Q. Tao, *Heat Transfer*, Higher Education Press, Beijing, China, Third Edition, 1998.
[26] Y. L. Zhao, R. Zhang, M. Qiu, and C. C. Duan, "Thermal mechanical coupling analysis of spherical plain bearings with woven liners," *Bearing*, no. 8, pp. 37–42, 2017.